Neu3 neuraminidase induction triggers intestinal inflammation and colitis in a model of recurrent human food-poisoning

Won Ho Yang[a,b,c,d,1] (ID), Julia S. Westman[a,b,c], Douglas M. Heithoff[a,c], Markus Sperandio[e] (ID), Jin Won Cho[d] (ID), Michael J. Mahan[a,c] (ID), and Jamey D. Marth[a,b,c,1]

[a]Center for Nanomedicine, University of California, Santa Barbara, CA 93106; [b]Infectious and Inflammatory Diseases Research Center, Sanford Burnham Prebys Medical Discovery Institute, La Jolla, CA 92037; [c]Department of Molecular, Cellular, and Developmental Biology, University of California, Santa Barbara, CA 93106; [d]Glycosylation Network Research Center and Department of Systems Biology, College of Life Science and Biotechnology, Yonsei University, Seoul 03722, Republic of Korea; and [e]Walter Brendel Center for Experimental Medicine, Institute of Cardiovascular Physiology and Pathophysiology, Ludwig Maximilian's University, 80539 Munich, Germany

Intestinal inflammation is the underlying basis of colitis and the inflammatory bowel diseases. These syndromes originate from genetic and environmental factors that remain to be fully identified. Infections are possible disease triggers, including recurrent human food-poisoning by the common foodborne pathogen *Salmonella enterica* Typhimurium (*ST*), which in laboratory mice causes progressive intestinal inflammation leading to an enduring colitis. In this colitis model, disease onset has been linked to Toll-like receptor-4–dependent induction of intestinal neuraminidase activity, leading to the desialylation, reduced half-life, and acquired deficiency of anti-inflammatory intestinal alkaline phosphatase (IAP). Neuraminidase (Neu) inhibition protected against disease onset; however, the source and identity of the Neu enzyme(s) responsible remained unknown. Herein, we report that the mammalian Neu3 neuraminidase is responsible for intestinal IAP desialylation and deficiency. Absence of Neu3 thereby prevented the accumulation of lipopolysaccharide-phosphate and inflammatory cytokine expression in providing protection against the development of severe colitis.

colitis | neuraminidase | inflammation

Colitis spanning the human inflammatory bowel diseases (IBDs) are debilitating and often life-threatening syndromes that arise from a combination of genetic and environmental factors (1–5). Environmental factors including antibiotics, smoking, stress, diet, and hygiene are thought to contribute to the incidence and elevation of IBD among various human populations (6, 7). Enteropathogen infections have also been considered as possible environmental triggers of disease (8–10). Various microbial infections typically occur during the lifespan of humans, which are often mild in severity and resolve without clinical intervention. Mild food-poisoning is an example, and in this regard, we previously developed a mouse model of recurrent nonlethal human food-poisoning using oral low-titer nonlethal infections of the bacterial pathogen *Salmonella enterica* Typhimurium (*ST*), a major cause of human foodborne illness leading to morbidity and mortality (11). Host elimination of the pathogen occurs in this model and is followed by recovery time prior to subsequent infection. Intestinal inflammation increases following each infection with the development of an enduring colitis that persists following the cessation of infections (12). Disease signs are similar to human ulcerative colitis.

Intestinal neuraminidase (Neu) activity is induced and required for the pathogenesis in this recurrent food-poisoning model of colitis. Neuraminidases, also known as sialidases, cleave sialic acids from glycan linkages of proteins and lipids and are encoded by the genomes of diverse organisms. However, the *ST* pathogen does not encode neuraminidase activity (13). Elevated Neu activity must come from another source among the host and the intestinal microbiota. With increased Neu activity, sialic acid linkages are hydrolyzed from intestinal glycoproteins including nascent intestinal alkaline phosphatase (IAP), resulting in reduced IAP half-life and leading to an acquired IAP deficiency. Oral high-dose administration of the viral neuraminidase (Neu) inhibitor Zanamivir blocked the induction of intestinal Neu activity, maintained IAP sialylation and abundance, and prevented disease (12).

IAP is an anti-inflammatory enzyme synthesized in the secretory pathway exclusively by duodenal enterocytes of the small intestine (14) where it is released into the lumen and diffuses throughout the lower intestinal tract. Among its activities, IAP dephosphorylates the lipopolysaccharide-phosphate (LPS-P) endotoxin produced by gram-negative bacteria residing primarily in the colon (15–17). IAP thereby detoxifies LPS-P as dephosphorylated forms of LPS do not activate the Tlr4 complex (18). Oral IAP augmentation or Zanamivir treatment each blocked the rise in LPS-phosphate levels and the resulting Tlr4-dependent colitis (12). Zanamivir's mechanism of protection was unclear, however, as it may have inhibited the activities of multiple neuraminidases produced by commensal microbes and host cells.

Discovering the identity of the Neu enzyme(s) responsible for pathogenesis is necessary to define the molecular pathway more fully for identifying approaches to therapeutic intervention. There

Significance

The environmental triggers of human colitis are unknown, while current treatments have limited efficacy. To find better therapies, various animal models of colitis have been investigated including studies of inborn genetic defects and chemical toxin ingestion. However, such models do not appear to identify common triggers of disease among human populations. We recently developed a recurrent food-poisoning model of colitis involving the *Salmonella* bacterial pathogen, a major source of human foodborne illness, and discovered that repeated infections over the adult lifespan cause a progressive intestinal inflammation that leads to a severe and enduring colitis. We have identified the Neu3 neuraminidase as essential in disease onset and provide rationale for the development of Neu3 inhibitors to prevent and treat colitis.

MEDICAL SCIENCES

are multiple neuraminidases produced by various commensal microbes in the lumen of the intestinal tract including the colon (19). Among mammalian genomes, four Neu genes have been identified (*Neu1* to *Neu4*), and each Neu protein differs in subcellular localization and enzymatic properties (20, 21). Among possibilities, the induction of host *Neu3* RNA was detected in the small intestine in response to *ST* infection and LPS-P administration (12). In addition, Neu3 induction was found to be dependent upon Tlr4 (12), suggesting the possibility that host Neu3 is a proinflammatory mediator of Tlr4 activation by LPS-P in triggering the onset of colitis. We have therefore investigated this hypothesis among Neu3-deficient mice in the context of a mouse model of recurrent human food-poisoning by the bacterial *ST* pathogen.

Results

Neu3 Is Responsible for IAP Desialylation and Deficiency. We investigated mice previously produced with homozygous null mutations in the *Neu3* allele, which are well tolerated with normal animal development and the absence of intestinal inflammation or spontaneous disease (12, 22). At 8 wk of age, cohorts of wild-type (WT) and *Neu3*-null littermates were inoculated by gastric intubation with 2×10^3 colony-forming units (cfu) of *ST* every 4 wk for 6 consecutive months as previously described (12). Among littermates of

both genotypes, *ST* was detected transiently as expected in the small intestine and a subset of lymphoid tissues but was reduced to undetectable levels in the host by 3 wk postinfection with all animals surviving long term (*SI Appendix*, Fig. S1). We detected Neu3 protein induction on the surface of the small intestinal epithelium among WT mice receiving *ST* infections, by comparison, *Neu3*-null cohorts lacked any measurable Neu3 antigen among uninfected and postinfection tissue samples (Fig. 1*A*). The absence of Neu3 protein was linked to a significant reduction in Neu activity measured throughout the duration of study (Fig. 1*B*). Although some Neu activity induction was detected in the small intestine, it was about a third of the level compared to Neu induction measured among infected WT littermates.

Alkaline phosphatase (AP) activity was measured using small intestinal tissue and luminal content extracts. We observed a significant decline in AP activity during the course of recurrent *ST* infections; while in contrast, Neu3-null littermates retained normal levels of AP activity in these compartments (Fig. 1*C*). The AP activity measurements were closely linked to IAP protein levels, which were similarly reduced while no change occurred in IAP RNA levels (Fig. 1 *D* and *E*). These findings indicate that Neu3 function is responsible for IAP deficiency in this recurrent food-poisoning model
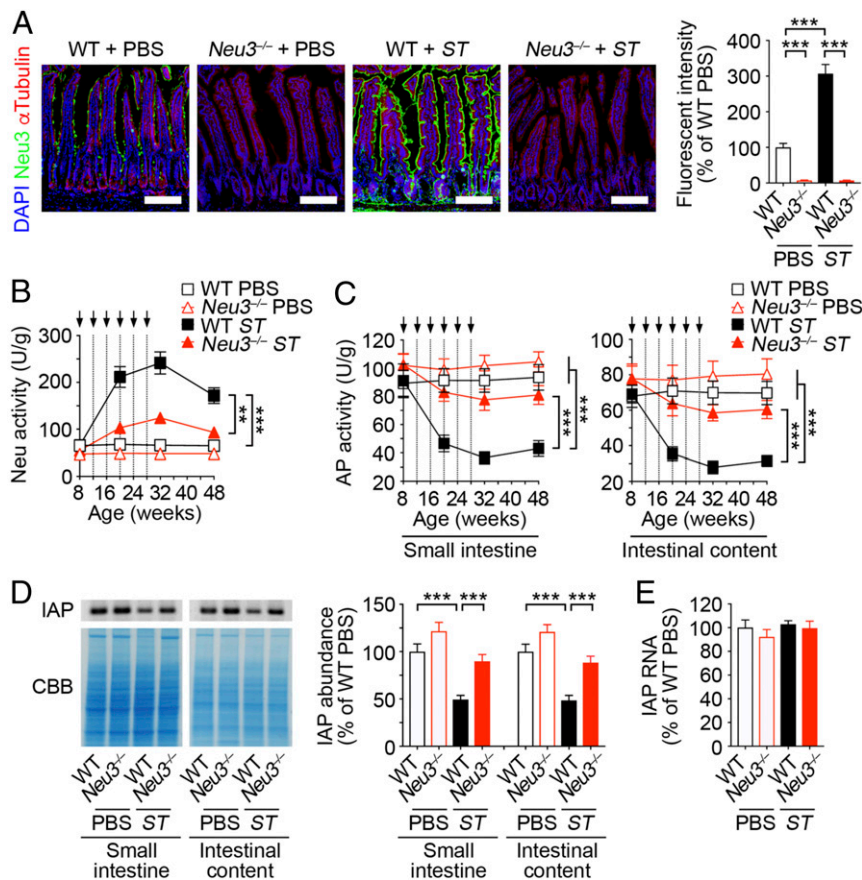
Fig. 1. Neu3 neuraminidase in the regulation of IAP expression. (*A*) In situ localization of Neu3 protein in tissue sections of littermates of indicated genotypes and conditions at 20 wk of age prior to the fourth recurrent *ST* infection or PBS control treatment. Neu3 protein is visualized in the duodenum of the small intestine using anti-Neu3 antibodies (green). DNA is stained with DAPI (blue). Quantitation was analyzed from 10 fields of view of tissue sections analyzed each from individual mice including littermates of indicated genotypes and conditions. (Scale bars, 100 μm.) (*B*) Neuraminidase (Neu) activity measured from total tissue homogenates of the small intestine during the course of recurrent *ST* infections (arrows). (*C*) AP activity levels measured from homogenates of small intestine tissue and intestinal luminal content during the course of recurrent *ST* infections (arrows). (*D*) Immunoblot analysis of IAP protein abundance at 20 wk of age prior to the fourth *ST* infection. (*E*) IAP mRNA expression quantified in small intestine tissue at 20 wk of age prior to the fourth *ST* infection. Data shown are representative from analyses of six to eight individual mice including littermates of each genotype and treatment condition and are presented as means ± SEM; **$P < 0.01$; ***$P < 0.001$.

of colitis and may do so by determining the rate of nascent IAP desialylation and endocytic clearance.

The glycan linkages attached to the IAP glycoprotein isolated from small intestine tissue were analyzed using lectins including galactose-binding *Erythrina cristagalli* agglutinin (ECA) and *Ricinus communis* agglutinin (RCA-I), the unsialylated Core 1 O-glycan-binding peanut agglutinin (PNA), the less selective α2-3 sialic acid-binding *Maackia amurensis* lectin II (MAL-II), and the highly selective α2-6 sialic acid-binding *Sambucus nigra* agglutinin (SNA). Significantly increased galactose exposure was measured comparing ECA and RCA lectin binding to IAP, while no differences in SNA binding to IAP were detected (Fig. 2*A*). The small but significant reduction in MAL-II lectin binding detected may reflect MAL-II binding to other glycan linkages or the possibility that Neu3 does not hydrolyze all α2-3 sialic acid linkages on IAP. These findings were similar to histological results of lectin binding to the epithelium of the small intestine with the exception of increased SNA binding in situ measured among *Neu3*-null littermates (*SI Appendix*, Fig. S2). This indicates that Neu3 is likely also involved in the desialylation of other epithelial glycoproteins that are modified by α2-6 sialic acid linkages. The desialylation of IAP in response

to recurrent *ST* infections was virtually abolished by Neu3 deficiency indicating that Neu3 induction is responsible for the desialylation of IAP.

Whether IAP desialylation by Neu3 causes IAP deficiency by diminishing IAP synthesis and trafficking to the cell surface or by reducing nascent cell-surface IAP half-life was investigated. Ex vivo primary enterocyte cultures were analyzed for IAP biosynthesis, trafficking to the cell surface, and cell-surface half-life in the presence and absence of prior *ST* infections. IAP synthesis and trafficking to the cell surface were unimpeded by Neu3 deficiency (Fig. 2*B*). In contrast, IAP half-life at the enterocyte cell surface was significantly reduced by a Neu3-dependent endocytic mechanism (Fig. 2 *C* and *D*). Neu3 induction increased the rate of nascent IAP desialylation and internalization prior to IAP release into the lumen, reducing IAP half-life at the cell surface in causing IAP deficiency.

Reduced Levels of LPS-P, Inflammatory Cytokines, and Leukocyte Infiltration with Normalization of Commensal *Enterobacteriaceae*. Elevated levels of LPS-P are also linked to disease onset and progression in this recurrent food-poisoning model of colitis (12). Among Neu3-deficient mice, the abundance of LPS-P per LPS mass in the
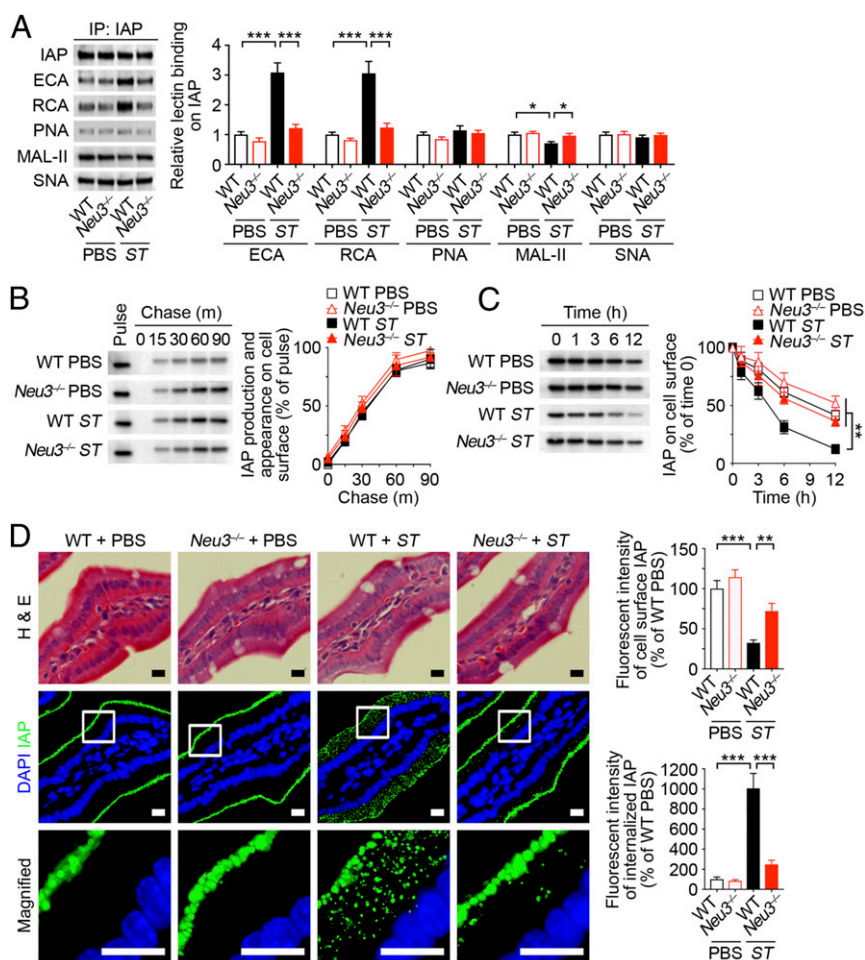
Fig. 2. Analyses of Neu3 involvement in IAP biosynthesis, desialylation, and half-life. (*A*) Lectin binding analyses using an ELISA format to compare glycan linkages attached to IAP isolated by immunoprecipitation from small intestine tissue at 20 wk of age prior to the fourth recurrent *ST* infection (*n* = 8 individual mice including littermates of each genotype and treatment condition). (*B* and *C*) Pulse–chase and cell-surface half-life analyses of IAP produced by cultured primary enterocytes isolated from WT and *Neu3*-null littermates at 20 wk of age prior to the fourth *ST* infection (*n* = 6 individual mice including littermates of each genotype and treatment condition). (*D*) In situ localization of IAP protein in sequential tissue sections of the duodenum of the small intestine stained with either hematoxylin/eosin (H&E) or fluorescent antibodies to IAP (green) at 20 wk of age prior to the fourth *ST* infection. A representative result is shown in measurements of IAP associated with the cell surface or internalized compared among 10 fields of view (*n* = 8 individual mice including littermates of each genotype and treatment condition). (Scale bars, 10 μm.) Data are presented as means ± SEM; *$P < 0.05$; **$P < 0.01$; ***$P < 0.001$.

Yang et al.
Neu3 neuraminidase induction triggers intestinal inflammation and colitis in a model of recurrent human food-poisoning

PNAS | 3 of 8
https://doi.org/10.1073/pnas.2100937118

www.manaraa.com

colon was reduced to almost normal in contrast to findings among WT cohorts retaining Neu3 function (Fig. 3A). Increased levels of total LPS that can further contribute to LPS-P levels may be ascribed to an increase of gram-negative *Enterobacteriaceae* that account for an increase of commensal bacterial load measured by bacterial 16S RNA probes compared to luminal content mass. Neu3 deficiency normalized levels of total LPS, *Enterobacteriaceae*, and commensal bacterial abundance (Fig. 3 A and B). In addition, RNA levels of multiple proinflammatory and immune regulatory cytokines were measured in colon tissue. All cytokines assayed were found to be induced by recurrent *ST* infections while induction was significantly reduced among Neu3-null mice throughout the course of study, including chemokine ligand-5, interleukin-1β, tumor necrosis factor-α, interferon-γ, interleukin-10, and transforming growth factor-β (Fig. 3C). In concordance with these findings, we detected significantly reduced leukocyte infiltration involving T cells (CD3ε$^+$), polymorphonuclear leukocytes including neutrophils (Gr1$^+$), and monocyte/macrophage lineages (F4/80$^+$) (Fig. 3D). These findings reveal that elevated Neu3 activity is a major factor causing the progressive elevation of inflammatory and immune regulatory cytokines.

Neu3 Deficiency Provides Protection against the Onset and Progression of Colitis. Visual, anatomical, and histological signs of colitis develop in response to recurrent *ST* infections as scored among intact animals and intestinal tissues. We analyzed colon tissue for histopathological markers including infiltrating leukocytes, epithelial layer discontinuities (erosion of the mucin barrier), and numbers of goblet cells. Neu3 deficiency significantly reduced the frequency of appearance of these disease signs (Fig. 4A). Cohorts undergoing recurrent *ST* infections were further monitored for body weight, colon length, and frequencies of diarrhea and fecal blood (Fig. 4 B–E). By these metrics also, Neu3 deficiency was highly protective and reduced or eliminated disease signs of colitis. In comparing colitis caused by dextran sulfate sodium (DSS) ingestion, there was no effect of Neu3 function on DSS-induced colitis (*SI Appendix*, Fig. S3) indicating the involvement of different pathogenic mechanisms.

Discussion

The mammalian Neu3 neuraminidase is required for the development of colitis in a mouse model of recurrent human food-poisoning involving repeated transient *ST* infections during the adult lifespan. This regimen causes a progressive and enduring colitis linked to induction of neuraminidase activity in the small intestine contributed primarily by Neu3. A minor fraction of Neu activity was Neu3 independent; however its effect on IAP sialylation and regulation was negligible. Neu3 deficiency alone was sufficient to maintain the sialylation of nascent IAP and normalize IAP half-life at the enterocyte cell surface prior to IAP release into the lumen. In turn, the retention of normal IAP abundance in the intestinal lumen of *Neu3*-null mice was linked to lower levels of the proinflammatory IAP substrate LPS-P in the colon with significant reductions of inflammatory cytokine RNA levels, leukocyte recruitment, and epithelial barrier erosion. This disease pathway points to the profound impact of factors produced in the small intestine upon processes required in the colon. The rise in bacterial load in the colon matched the overgrowth of *Enterobacteriaceae*, a finding commonly observed among models of intestinal inflammation and colitis (23). Therefore, the measured increase in abundance of LPS-P in the colon is likely due to a combination of reduced IAP activity and increased numbers of gram-negative *Enterobacteriaceae*. What causes the bloom of *Enterobacteriaceae* remains to be established. Nevertheless, LPS-P is permeable to the mucosal barrier; therefore, higher LPS-P levels are likely to generate increased Tlr4-dependent inflammation required for disease onset and progression in this recurrent food-poisoning model of colitis (12).

The mechanism triggering colitis by Neu3 induction appears distinct from colitis caused by ingestion of the chemical toxin DSS and its modulation by various acquired and genetic factors, some of which include other glycan linkages (24–28). DSS ingestion is toxic to epithelial cells and remains a convenient rapid approach to model the pathogenesis and treatment of colitis (29). This toxin generates colonic lesions by disrupting the mucosal barrier causing increased intestinal permeability that precedes inflammation and colitis. Interestingly, not all colitis models generate the same cytokine expression profiles, particularly among the immune regulatory factors, which may indicate the participation of different inflammatory signaling pathways (30–34). In comparing DSS-induced colitis, Tlr4 function appears protective in some contexts (35). This may reflect the importance of Tlr4 in acute severe injury by rapidly mobilizing innate immune cells and promoting tissue repair. In contrast, Tlr4 is required for the development of colitis due to repeated low-titer nonlethal ST infections in this model of recurrent human food-poisoning (12). Inflammation in this latter model increases slowly over the adult lifespan with chronically elevated LPS-P levels causing tissue damage and leading to an enduring colitis that remains after the cessation of repeated infections. As such, these two colitis models reveal significant disparity in the pathogenic mechanisms involved and in the rationales for disease prevention and treatment.

Endogenous desialylation by mammalian Neu enzymes has been linked to regulating the half-lives of multiple secreted and cell-surface glycoproteins (36). Multiple pathogens target this endocytic lectin-ligand clearance mechanism in gaining an advantage over the host as altering the half-lives of secreted bioactive proteins is among the most rapid means of regulating their function (12, 37). Increased Neu activity accelerates the rate of removal of sialic acids from nascent glycoproteins with increased exposure of underlying galactose ligands of endocytic lectin receptors including the prototypical hepatocyte Ashwell–Morell receptor (38–40). There are over a hundred lectin receptors thus far identified in the mammalian genome, and their glycoprotein ligand repertoires are mostly unknown (41). It is possible that duodenal enterocytes express one or more galactose-binding endocytic lectins that internalize IAP following its desialation by Neu3. Conversely, there may exist other lectins on the surface of enterocytes, such as one or more Siglecs typically found on immune cells (42) that may bind sialylated IAP in extending its half-life at the cell surface. Our findings support the rationale for future investigations to identify the lectin receptor(s) involved.

Neu3-dependent desialylation of IAP involved the hydrolysis of α2-3 linked sialic acids, which are among the most prevalent if not only sialic acid linkage type attached to the glycans of IAP (12). This is consistent with previous studies where ST3Gal6 was found to be responsible for IAP sialylation in protecting against acquired IAP deficiency and the onset of spontaneous colitis (12). This was surprising as Neu3 activity in vitro indicates a strong preference for sialylated glycolipid substrates (43). The rate of desialylation of nascent IAP glycoprotein in vivo by Neu3 is nevertheless inversely proportional to is nevertheless IAP IAP half-life and abundance. Interestingly, the increase in SNA binding among *Neu3*-null duodenal epithelial cells indicates that Neu3 also desialylates and may similarly modulate multiple glycoproteins including those identified previously (12) and may thereby cause other changes to glycoconjugate structure and membrane organization (44).

Neu3 induction following oral *ST* infection links an inflammatory mechanism to a chronic environmental trigger that may explain the origin of colitis among some human populations. Increased levels of intestinal Neu3 and reduced levels of IAP have been observed in human colitis while inborn genetic deficiency of IAP in humans causes IBD, together providing support for oral IAP augmentation strategies in clinical trials (45–49). Neu inhibition provides an equally efficacious approach in the mouse and possibly in humans (12). Neu3 inhibition may be also therapeutic in cancers of
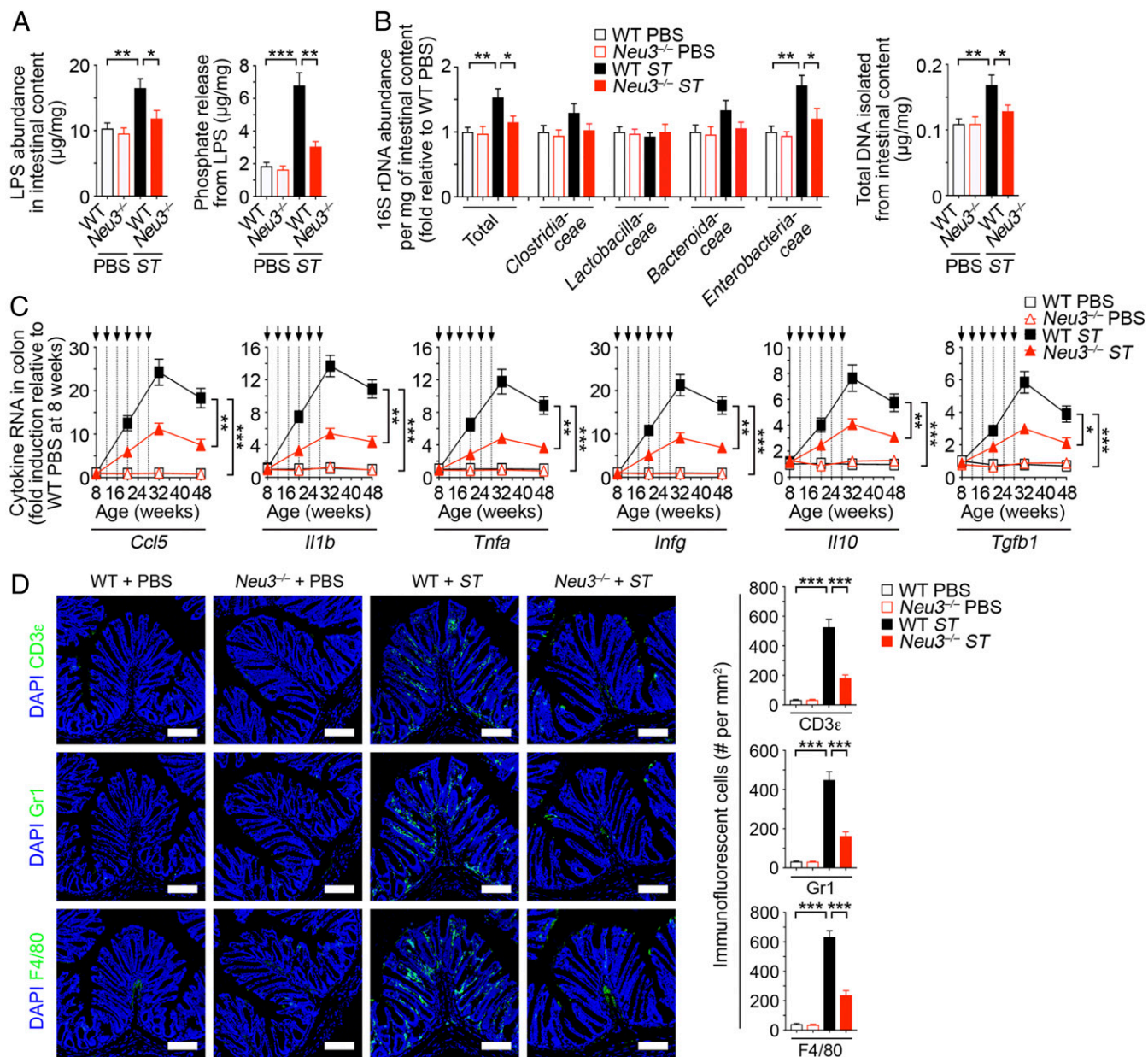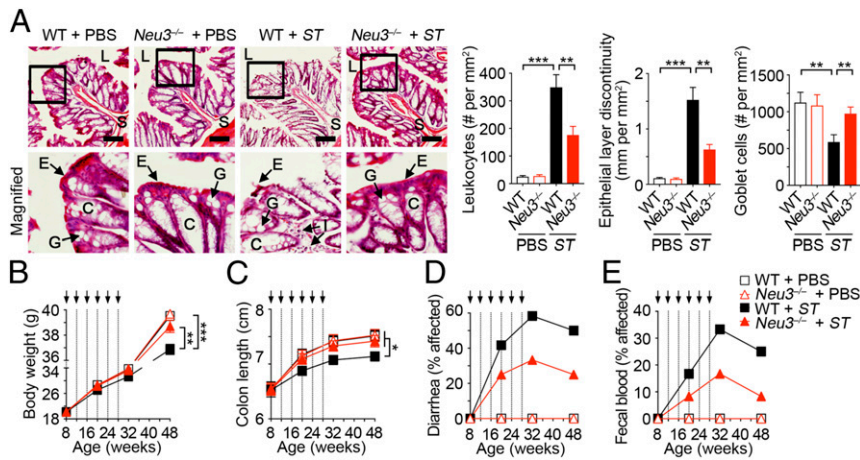
Fig. 3. Neu3 function in modulating intestinal LPS, inflammatory cytokines, leukocyte infiltrates, and commensal microbiota. (*A*) Abundance of total LPS and LPS-P were compared from the intestinal content of mice at 20 wk of age prior to the fourth *ST* infection ($n = 6$ individual mice including littermates of each genotype and treatment condition). (*B*) Intestinal microbiota comparisons and total DNA levels obtained from 1 mg intestinal contents from individual mice at 20 wk of age prior to the fourth *ST* infection and analyzed using common and selective bacterial 16S ribosomal probes ($n = 8$ mice including littermates of each genotype and treatment condition). (*C*) Inflammatory cytokine mRNA expression in isolated colon tissue ($n = 16$ individual mice including littermates of each genotype and treatment condition). (*D*) Serial sections of colon isolated from WT and *Neu3*-null littermates at 20 wk of age prior to the fourth *ST* infection were analyzed using antibodies to detect T cells (CD3ε), polymorphonuclear leukocytes including neutrophils (Gr1), and monocytes/macrophages (F4/80). Representative results are shown with quantified levels of leukocyte infiltration measured from 10 fields of view ($n = 4$ mice including littermates of each genotype and treatment condition). (Scale bars, 100 μm.) Data are presented as means ± SEM; *$P < 0.05$; **$P < 0.01$; ***$P < 0.001$.

the colon, renal, and prostate tissues; moreover, Neu3 deficiency in mice resulted in fewer colitis-associated colonic tumors (22, 50–52). In the context of the colitis model studied herein, the onset of disease signs with tissue damage are more complex than can be explained simply by elevated LPS-P abundance and Tlr4 activation. Dysbiosis among the commensal microbiota and the erosion of the protective mucin barrier are hallmarks of colitis in mice and humans, yet they cannot be explained at present by the currently known functions of Neu3, IAP, and Tlr4, indicating that other pathogenic mechanisms remain to be identified. Nevertheless, our identification of Neu3 as an essential component of pathogenesis suggests its potential value as a selective upstream target for inhibition in the prevention and treatment of intestinal inflammation and colitis.

Materials and Methods

Yang et al.
Neu3 neuraminidase induction triggers intestinal inflammation and colitis in a model of recurrent human food-poisoning

PNAS | 5 of 8
https://doi.org/10.1073/pnas.2100937118

www.manaraa.com

Fig. 4. Neu3 contribution to the onset and progression of colitis. (*A*) Hematoxylin and eosin–stained colon sections isolated at 48 wk of age (20 wk following the last *ST* infection at 28 wk of age) were analyzed for histological signs of inflammation and colitis. L, intestinal lumen; E, epithelial layer; C, crypt; G, goblet cell; S, submucosa; I, infiltrating leukocyte. Numbers of leukocytes, frequencies of detection of epithelial mucin barrier discontinuities (mucin barrier erosion), and goblet cell numbers were quantified from 12 fields of view each from four independent mice including littermates of each genotype and treatment condition. Representative sections are shown. (Scale bars, 100 μm.) (*B*–*E*) Body weight (*n* = 10), colon length (*n* = 32), frequency of diarrhea (*n* = 12), and frequency of fecal blood detected (*n* = 12) were plotted throughout 48 wk of age of adult life in the course of recurrent *ST* infections (arrows) and following their cessation among the indicated (*n*) number of mice of each genotype and condition. Data are presented as means ± SEM; *$P < 0.05$; **$P < 0.01$; ***$P < 0.001$.

Burnham Prebys Medical Discovery Institute approved the mouse studies undertaken herein.

Bacterial Strains and Infection Protocols. MT2057, a kanamycin-resistant derivative of *Salmonella enterica* subsp. *enterica* serovar Typhimurium reference strain ATCC 14028 (Centers for Disease Control 6516-60) was used as previously described (12, 53). Adult 8-wk-old mice were infected with *ST* (2×10^3 cfu) via gastric intubation at 4-wk intervals successively up to five times during adult life. Mice were weighed biweekly and further assessed for overt signs including the presence of diarrhea and fecal blood (occult fecal blood positive, Beckman Coulter) as previously described (12, 54).

Measurements of Bacterial Titers. To measure bacterial cfu, mice were euthanized and then samples of tissues and blood were obtained using aseptic technique. Peyer's Patch, mesenteric lymph node, spleen, small intestine, colon, and liver (0.1 g of each) were homogenized in 1 mL sterile phosphate-buffered saline (PBS) using a sterile pestle, and 200 μl tissue homogenates were plated on Luria–Bertani (LB) agar plates supplemented with kanamycin. Intestinal content including feces (0.1 g) was homogenized in 200 μl sterile PBS using a sterile pestle, and whole homogenates were plated on LB agar plates supplemented with kanamycin (50 μg/mL) to calculate cfu/g. Blood collected from the tail vein (100 μl) was serially diluted in 100 μl sterile PBS in PBS and plated on LB agar plates supplemented with kanamycin (50 μg/mL) to calculate cfu/mL. The plates were incubated in an incubator at 37 °C for 24 h, and bacterial cfu/g in tissue or tissue content and cfu/mL in blood were calculated.

Histology. Mouse intestinal tissues were fixed in 10% buffered formalin (Sigma-Aldrich), transferred to 30% sucrose/PBS, and embedded in Tissue-Tek optimal cutting temperature compound (Sakura Finetek). Next, 3-μm frozen sections were prepared and stained with hematoxylin and eosin (Sigma-Aldrich) or incubated with 1 μg/mL antibodies to one or more molecules including Neu3 (M-50, Santa Cruz Biotechnology), αTubulin (P-16, Santa Cruz Biotechnology), CD3ε (M-20, Santa Cruz Biotechnology), Gr-1 (M-66, Santa Cruz Biotechnology), F4/80 (M-300, Santa Cruz Biotechnology), or 1:1,000 dilution of IAP-specific antiserum (55) or 5 μg/mL of biotinylated lectins including ECA, RCA, PNA, MAL-II, or SNA (Vector Laboratories). Neu3, IAP, Gr-1, and F4/80 were visualized with 0.4 μg/mL fluorescein isothiocyanate (FITC)-conjugated goat anti-rabbit IgG secondary antibodies (Santa Cruz Biotechnology); CD3ε was visualized with 0.4 μg/mL FITC-conjugated rabbit anti-goat IgG secondary antibodies (Santa Cruz Biotechnology); αTubulin was visualized with 0.4 μg/mL Texas Red-conjugated rabbit anti-goat IgG secondary antibodies (Santa Cruz Biotechnology); and biotinylated lectins were visualized with 1 μg/mL FITC-conjugated streptavidin (Vector Laboratories). These primary antibody

or lectin incubations were performed at 4 °C overnight, and secondary antibody or streptavidin incubations were performed at room temperature for 1 h. Analyses by microscopy was performed using a TissueGnostics workstation equipped with Zeiss AxioImager Z1, Hamamatsu C13440-20C camera, PixeLINK PL-D673CU camera, and Lumen Dynamics X-Cite XLED1 illuminator. Images collected were analyzed using TissueFAXS (version 3.5), TissueQuest (version 4.0), and HistoQuest software (version 4.0) (TissueGnostics USA Ltd.).

Neuraminidase Activity and Inhibition. Neuraminidase activity was measured in tissue extracts in radioimmunoprecipitation assay (RIPA) buffer (50 mM Tris HCl [pH 7.6], 150 mM NaCl, 1 mM EDTA, 1% Nonidet P-40, 1% sodium deoxycholate, and 0.1% sodium dodecyl sulfate [SDS]) supplemented with complete protease inhibitor mixture per instructions (Roche) using the Amplex Red Neuraminidase Assay Kit according to the manufacturers' instructions (Molecular Probes).

mRNA Preparation and Quantification by Real-Time PCR. Total RNA was isolated from tissues using TRIzol (Invitrogen) and subjected to reverse transcription (RT) using SuperScript III (Invitrogen). Real-time qPCR was performed using Brilliant SYBR Green Reagents with the Mx3000P QPCR System (Stratagene). Primers used for real-time PCR in the mouse were as follows: CCL5-RT-F (5′-TCGTGTTTGTCACTCGAAGG-3′), CCL5-RT-R (5′-CTAGCT-CATCTCCAAATAGT-3′), IL-1β-RT-F (5′-GCCCATCCTCTGTGACTCAT-3′), IL-1β -RT-R (5′-AGGCCACAGGTA-TTTTGTCG-3′), TNFα-RT-F (5′-CATCTTCTCAAAATTCGAGT-3′), TNFα-RT-R (5′-TTT-GAGATCCATGGCCT-3′), IFNγ-RT-F (5′-ACTGGCAAA-AGGATGGTGAC-3′), IFNγ-RT-R (5′-GTTGCTGATGGCCTGATTGT-3′), IAP-RT-F (5′-CTCATCTCCAACATG-GAC-3′), IL-10-RT-F (5′-GTGAAGACTTTCTTTGAAACA-AAG-3′), IL-10-RT-R (5′-CTGCTCCACTGCCTTGCTCTTATT-3′), TGFβ1-RT-F (5′- CCC-GAAGCGGACTACTAT-GCT-3′), TGFβ1-RT-R (5′- GTTTTCTCATAGATGGCGTTGTTG-3′), IAP-RT-R (5′-TGC-TTAGCACTTTCACGG-3′), GAPDH-RT-F (5′-TGGTGA-AGGTCGGTGTGAAC-3′), and GAPDH-RT-R (5′-AGT-GATGGCATGGACTGTGG-3′). Messenger RNA (mRNA) levels were normalized to expression of GAPDH mRNA.

Immunoprecipitation, Immunoblotting, and Lectin Blotting. Tissue samples were homogenized in RIPA buffer supplemented with complete protease inhibitor mixture per instructions (Roche) and incubated overnight at 4 °C on a rotating wheel with 1:100 dilution of IAP-specific antiserum (55), followed by 2 h of incubation in the presence of protein A/G PLUS agarose (Santa Cruz Biotechnology). Immunoprecipitates were washed five times with RIPA buffer and eluted with SDS sample buffer. Protein samples eluted were subjected to SDS-polyacrylamide gel electrophoresis (PAGE), transferred to nitrocellulose membranes, and incubated with 3% bovine serum albumin (BSA) in Tris-buffered saline (TBS). They were then analyzed by immuno-blotting using 1:1,000 dilution of IAP-specific antiserum or by lectin blotting with

www.manaraa.com

horseradish peroxidase (HRP)-conjugated ECA (0.5 μg/mL), RCA (0.1 μg/mL), PNA (1 μg/mL), MAL-II (0.2 μg/mL), or SNA (0.1 μg/mL) (EY Laboratories). Signals detected by chemiluminescence (GE Healthcare) were analyzed by integrated optical density using Labworks software (UVP Bioimaging Systems). Parallel protein samples were visualized with Coomassie brilliant blue G250 staining (Bio-Rad).

ELISA. Enzyme-linked immunosorbent assay (ELISA) plates (Nunc) were coated with 1:1,000 dilution of IAP-specific antiserum and blocked by incubation at room temperature for 1 h with 5% BSA in PBS (Jackson ImmunoResearch). To generate biotinylated antigens, 500 μl total protein extracts isolated from mouse tissue (1 mg/mL) were incubated with 500 μl sulfo-NHS-LC-biotin (1 mg/mL) (Pierce Chemical) on ice for 2 h, and the biotinylation reaction was stopped with the addition of 15 mM glycine (pH 8.0; final concentration). After washing the ELISA plates, 20 μg biotinylated protein extract was added to each well and incubated at room temperature for 2 h. Antigens were detected following the addition of 1:5,000 dilution of HRP-streptavidin (BD Biosciences) and 3,3′,5,5′ tetramethylbenzidine (TMB, Sigma-Aldrich). Lectin binding was determined in parallel by the addition of HRP-conjugated ECA (0.5 μg/mL), RCA (0.1 μg/mL), PNA (1 μg/mL), MAL-II (0.2 μg/mL), or SNA (0.1 μg/mL) (EY Laboratories), followed by TMB, and changes in glycan linkages were detected by comparing lectin binding among identical amounts of biotinylated IAP (56). AP activity was measured using the p-nitrophenyl phosphate substrate (Sigma-Aldrich) as described (57).

Pulse–Chase and Cell-Surface Half-Life Analyses. Techniques as previously described (58) were used for pulse–chase measurements of IAP synthesis and trafficking among cultured primary enterocytes. Mouse enterocytes were isolated from the duodenum as previously described (59). The proximal duodenum was removed and flushed through with solution A (1.5 mM KCl, 96 mM NaCl, 27 mM sodium citrate, 8 mM KH_2PO_4, and 5.6 mM Na_2HPO_4) at room temperature. The duodenum was minced in an enzyme mixture (333 U/mL collagenase, 2.5 U/mL elastase, and 10 μg/mL DNase) in Hepes-buffered Krebs-Ringer solution (5 mM Hepes [4-(2-hydroxyethyl)-1-piperazineethanesulfonic acid, pH 7.4], 120 mM NaCl, 24 mM $NaHCO_3$, 4.8 mM KCl, 1.2 mM $MgSO_4$, 1.2 mM KH_2PO_4, 20 mM glucose, 1 mM $CaCl_2$) and incubated while shaking at 37 °C for 30 min. Cells were filtered through a 70-μm filter and washed twice in Dulbecco's Modified Eagle's Medium (DMEM) supplemented with 10% fetal calf serum, 1% β-mercaptoethanol, and 1% L-asparagine. Isolated enterocytes were washed twice with Hank's balanced salt solution (HBSS), then cultured with DMEM depleted of methionine (Gibco) with 10% fetal calf serum for 2 h at 37 °C. Pulse labeling was performed with 400 μCi/mL [^{35}S]-methionine for 10 min at 37 °C, and cells were then washed twice in ice-cold HBSS. Cells were lysed or returned to new media of above culture conditions containing 2 mM methionine for 15, 30, 60, or 90 min. Cells used in chase samples were washed twice with ice-cold PBS and incubated with 1 mg/mL sulfo-NHS-LC-biotin (Pierce Chemical) at 4 °C for 30 min. Biotinylation was stopped by three washes with 15 mM glycine in ice-cold PBS. Cells were homogenized in RIPA buffer, and biotinylated proteins were purified using immobilized monomeric avidin gel (Pierce). Eluates isolated in the presence of D-biotin (Pierce) for chase were incubated with IAP-specific antiserum. Immunoprecipitates were subjected to SDS-PAGE, and gels were fixed before drying and autoradiography at −70 °C for 3 to 7 d. For cell-surface IAP half-life analysis, enterocytes were washed twice with ice-cold PBS and biotinylated with sulfo-NHS-LC-biotin. Cells were further cultured at the indicated times and then homogenized in RIPA buffer, followed by immunoprecipitation using IAP-specific antiserum. IAP immunoprecipitates were subjected to SDS-PAGE, transferred to nitrocellulose membranes, and visualized with HRP-conjugated streptavidin.

LPS Phosphorylation. LPS was isolated as previously described (60) by the hot phenol–water method with minor modifications. Briefly, total intestinal contents were weighed, diluted 10-fold weight to volume in TBS, and homogenized. The soluble extract was then added to same volume of 99% phenol (Ambion), preheated to 65 °C, and incubated for 15 min at 65 °C. After cooling on ice, the samples were centrifuged at 10,000 × g for 10 min.

The aqueous phase was isolated, and residual phenol was removed by extracting with diethyl ether (Sigma-Aldrich). The diethyl ether phase was discarded, and the water phase containing the LPS was placed in a hood for 1 h to allow the remaining diethyl ether to evaporate. The above steps were repeated after treatment with proteinase K (Promega), RNase (Invitrogen), and DNase (Invitrogen). LPS preparations from indicated sources were quantified by the purpald assay as described previously (61). LPS preparations for comparative studies were indistinguishable by chromatography and silver staining (Bio-Rad). To compare the abundance of phosphate linked to LPS, phosphate release was measured by the malachite green phosphate assay (57). Briefly, purified calf IAP (10 U; Invitrogen) was incubated at pH 8.0 for 3 h at 37 °C with 1 mg LPS isolated from intestinal content. Free phosphate released was measured as a colored complex of phosphomolybdate and malachite green at 620 nm according to the manufacturer's instructions (BioAssay Systems).

Comparative Studies of Intestinal Microbiota. Total DNA was extracted from 1 mg intestinal content per individual mouse using QIAamp DNA Mini Kit according to the manufacturer's instructions (Qiagen). Total DNA was quantified and used as the template for real-time qPCR. A subset of commensal microbial populations was analyzed with Brilliant SYBR Green Reagents and the Mx3000P QPCR System (Stratagene). Oligonucleotide primers for total bacterial DNA were (Total-F-5′-GTGCCAGCMGCCGCGGTAA-3′, Total-R-5′-GACTACCAGGGTATCTAAT-3′; while those to measure individual populations included *Clostridiaceae*-F-5′-TTAACACAATAAGTWATCCACCT-GG-3′, *Clostridiaceae* -R-5′- ACCTTCCTCCGTTTTGTCAAC-3′; *Lactobacillaceae*-F-5′-AGCAGTAGGGAATCTTCC-3′, *Lactobacillaceae*-R-5′-CGCCACTGGTGTTCYT-CCATATA-3′; *Bacteroidaceae*-F-5′-CCAATGTGGGGGACCTTC-3′, *Bacteroidaceae*-R-5′-AACGCTAGCTACAGGCTT-3′; and *Enterobacteriaceae*-F-5′-CATTGACGT-TACCCGCAGAAGAAGC-3′, *Enterobacteriaceae*-R-5′-CTCTACGAGACTCAAG-CTTGC-3′) as described (62). Serial dilutions of total DNA were used to generate standard curves in acquiring each measurement. Relative levels of bacterial DNA obtained per mg of intestinal content from each mouse were calculated in plotting comparisons to WT littermates.

DSS-Induced Colitis. For studies in DSS-induced colitis, 12-wk-old mice were administered drinking water containing 4% DSS (molecular weight, 40,000 to 50,000; USB Corp.) ad libitum for 5 d and then returned to normal drinking water without DSS until the end of the experiment (day 14). Survival, body weight, stool consistency, the presence of occult blood, histology, and cytokine mRNA levels were determined. Stool scores were determined as follows: 0, well-formed pellets; 1, semiformed stools that did not adhere to the anus; 2, semiformed stools that adhered to the anus; and 3, liquid stools that adhered to the anus. Bleeding scores were determined as follows: 0, no blood as tested with hemocult (Beckman Coulter); 1, positive hemocult; 2, blood traces in stool visible; and 3, gross rectal bleeding as previously described (12).

Statistical Analysis. All data were analyzed as mean ± SEM unless otherwise indicated. Student's unpaired t test or one-way ANOVA with Tukey's multiple comparisons test with GraphPad Prism software (version 7.0) were used to determine statistical significance among multiple studies. P values of less than 0.05 were considered significant. Statistical significance was denoted by *$P < 0.05$, **$P < 0.01$, or ***$P < 0.001$.

Data Availability. All study data are included in the article and/or *SI Appendix*.

1. D. B. Graham, R. J. Xavier, Pathway paradigms revealed from the genetics of inflammatory bowel disease. *Nature* **578**, 527–539 (2020).
2. W. E. Ek, M. D'Amato, J. Halfvarson, The history of genetics in inflammatory bowel disease. *Ann. Gastroenterol.* **27**, 294–303 (2014).
3. D. Knights, K. G. Lassen, R. J. Xavier, Advances in inflammatory bowel disease pathogenesis: Linking host genetics and the microbiome. *Gut* **62**, 1505–1510 (2013).
4. B. Khor, A. Gardet, R. J. Xavier, Genetics and pathogenesis of inflammatory bowel disease. *Nature* **474**, 307–317 (2011).
5. A. Kaser, S. Zeissig, R. S. Blumberg, Inflammatory bowel disease. *Annu. Rev. Immunol.* **28**, 573–621 (2010).
6. A. N. Ananthakrishnan *et al.*, Environmental triggers in IBD: A review of progress and evidence. *Nat. Rev. Gastroenterol. Hepatol.* **15**, 39–49 (2018).
7. D. S. Shouval, P. A. Rufo, The role of environmental factors in the pathogenesis of inflammatory bowel diseases: A review. *JAMA Pediatr.* **171**, 999–1005 (2017).
8. J. E. Axelrad, K. H. Cadwell, J. F. Colombel, S. C. Shah, Systematic review: Gastrointestinal infection and incident inflammatory bowel disease. *Aliment. Pharmacol. Ther.* **51**, 1222–1232 (2020).
9. A. Sonnenberg, Seasonal variation of enteric infections and inflammatory bowel disease. *Inflamm. Bowel Dis.* **14**, 955–959 (2008).

Yang et al.
Neu3 neuraminidase induction triggers intestinal inflammation and colitis in a model of recurrent human food-poisoning

PNAS | 7 of 8
https://doi.org/10.1073/pnas.2100937118
www.manaraa.com

MEDICAL SCIENCES

10. L. Eckmann, Animal models of inflammatory bowel disease: Lessons from enteric infections. *Ann. N. Y. Acad. Sci.* **1072**, 28–38 (2006).

11. GBD 2017 Non-Typhoidal Salmonella Invasive Disease Collaborators, The global burden of non-typhoidal Salmonella invasive disease: A systematic analysis for the Global Burden of Disease Study 2017. *Lancet Infect. Dis.* **19**, 1312–1324 (2019).

12. W. H. Yang et al., Recurrent infection progressively disables host protection against intestinal inflammation. *Science* **358**, eaao5610 (2017).

13. L. L. Hoyer, A. C. Hamilton, S. M. Steenbergen, E. R. Vimr, Cloning, sequencing and distribution of the *Salmonella typhimurium* LT2 sialidase gene, nanH, provides evidence for interspecies gene transfer. *Mol. Microbiol.* **6**, 873–884 (1992).

14. B. F. Hinnebusch et al., Enterocyte differentiation marker intestinal alkaline phosphatase is a target gene of the gut-enriched Kruppel-like factor. *Am. J. Physiol. Gastrointest. Liver Physiol.* **286**, G23–G30 (2004).

15. J. M. Bates, J. Akerlund, E. Mittge, K. Guillemin, Intestinal alkaline phosphatase detoxifies lipopolysaccharide and prevents inflammation in zebrafish in response to the gut microbiota. *Cell Host Microbe* **2**, 371–382 (2007).

16. I. Koyama, T. Matsunaga, T. Harada, S. Hokari, T. Komoda, Alkaline phosphatases reduce toxicity of lipopolysaccharides in vivo and in vitro through dephosphorylation. *Clin. Biochem.* **35**, 455–461 (2002).

17. K. Poelstra, W. W. Bakker, P. A. Klok, M. J. Hardonk, D. K. Meijer, A physiological function for alkaline phosphatase: Endotoxin detoxification. *Lab. Invest.* **76**, 319–327 (1997).

18. S. Bentala et al., Removal of phosphate from lipid A as a strategy to detoxify lipopolysaccharide. *Shock* **18**, 561–566 (2002).

19. Y. L. Huang, C. Chassard, M. Hausmann, M. von Itzstein, T. Hennet, Sialic acid catabolism drives intestinal inflammation and microbial dysbiosis in mice. *Nat. Commun.* **6**, 8141 (2015).

20. E. Monti, T. Miyagi, Structure and function of mammalian sialidases. *Top. Curr. Chem.* **366**, 183–208 (2015).

21. E. Monti et al., Sialidases in vertebrates: A family of enzymes tailored for several cell functions. *Adv. Carbohydr. Chem. Biochem.* **64**, 403–479 (2010).

22. K. Yamaguchi et al., Reduced susceptibility to colitis-associated colon carcinogenesis in mice lacking plasma membrane-associated sialidase. *PLoS One* **7**, e41132 (2012).

23. M. Y. Zeng, N. Inohara, G. Nuñez, Mechanisms of inflammation-driven bacterial dysbiosis in the gut. *Mucosal Immunol.* **10**, 18–26 (2017).

24. K. Bergstrom et al., Core 1- and 3-derived O-glycans collectively maintain the colonic mucus barrier and protect against spontaneous colitis in mice. *Mucosal Immunol.* **10**, 91–103 (2017).

25. Q. H. Sun et al., Enhanced O-linked glcnacylation in Crohn's disease promotes intestinal inflammation. *EBioMedicine* **53**, 102693 (2020).

26. X. Verhelst et al., Protein glycosylation as a diagnostic and prognostic marker of chronic inflammatory gastrointestinal and liver diseases. *Gastroenterology* **158**, 95–110 (2020).

27. A. M. Dias et al., Metabolic control of T cell immune response through glycans in inflammatory bowel disease. *Proc. Natl. Acad. Sci. U.S.A.* **115**, E4651–E4660 (2018).

28. H. Fujii et al., Core fucosylation on T cells, required for activation of T-cell receptor signaling and induction of colitis in mice, is increased in patients with inflammatory bowel disease. *Gastroenterology* **150**, 1620–1632 (2016).

29. D. D. Eichele, K. K. Kharbanda, Dextran sodium sulfate colitis murine model: An indispensable tool for advancing our understanding of inflammatory bowel diseases pathogenesis. *World J. Gastroenterol.* **23**, 6016–6029 (2017).

30. V. Bäcker, F. Y. Cheung, J. T. Siveke, J. Fandrey, S. Winning, Knockdown of myeloid cell hypoxia-inducible factor-1α ameliorates the acute pathology in DSS-induced colitis. *PLoS One* **12**, e0190074 (2017).

31. T. Kanda et al., Enterococcus durans TN-3 induces regulatory T cells and suppresses the development of dextran sulfate sodium (DSS)-induced experimental colitis. *PLoS One* **11**, e0159705 (2016).

32. J. Däbritz, L. M. Judd, H. V. Chalinor, T. R. Menheniott, A. S. Giraud, Altered gp130 signalling ameliorates experimental colitis via myeloid cell-specific STAT3 activation and myeloid-derived suppressor cells. *Sci. Rep.* **6**, 20584 (2016).

33. Y. Shi, P. Rupa, B. Jiang, Y. Mine, Hydrolysate from eggshell membrane ameliorates intestinal inflammation in mice. *Int. J. Mol. Sci.* **15**, 22728–22742 (2014).

34. E. N. McNamee et al., Interleukin 37 expression protects mice from colitis. *Proc. Natl. Acad. Sci. U.S.A.* **108**, 16711–16716 (2011).

35. S. Rakoff-Nahoum, J. Paglino, F. Eslami-Varzaneh, S. Edberg, R. Medzhitov, Recognition of commensal microflora by toll-like receptors is required for intestinal homeostasis. *Cell* **118**, 229–241 (2004).

36. W. H. Yang et al., An intrinsic mechanism of secreted protein aging and turnover. *Proc. Natl. Acad. Sci. U.S.A.* **112**, 13657–13662 (2015).

37. W. H. Yang et al., Accelerated aging and clearance of host anti-inflammatory enzymes by discrete pathogens fuels sepsis. *Cell Host Microbe* **24**, 500–513.e5 (2018).

38. P. K. Grewal et al., The Ashwell receptor mitigates the lethal coagulopathy of sepsis. *Nat. Med.* **14**, 648–655 (2008).

39. C. Deppermann et al., Macrophage galactose lectin is critical for Kupffer cells to clear aged platelets. *J. Exp. Med.* **217**, e20190723 (2020).

40. G. Ashwell, A. G. Morell, The role of surface carbohydrates in the hepatic recognition and transport of circulating glycoproteins. *Adv. Enzymol. Relat. Areas Mol. Biol.* **41**, 99–128 (1974).

41. M. E. Taylor, K. Drickamer, Mammalian sugar-binding receptors: Known functions and unexplored roles. *FEBS J.* **286**, 1800–1814 (2019).

42. P. R. Crocker, J. C. Paulson, A. Varki, Siglecs and their roles in the immune system. *Nat. Rev. Immunol.* **7**, 255–266 (2007).

43. T. Wada et al., Cloning, expression, and chromosomal mapping of a human ganglioside sialidase. *Biochem. Biophys. Res. Commun.* **261**, 21–27 (1999).

44. M. A. Howlader et al., Neuraminidase-3 is a negative regulator of LFA-1 adhesion. *Front Chem.* **7**, 791 (2019).

45. J. J. Miklavcic et al., Increased catabolism and decreased unsaturation of ganglioside in patients with inflammatory bowel disease. *World J. Gastroenterol.* **21**, 10080–10090 (2015).

46. M. Lukas et al., Exogenous alkaline phosphatase for the treatment of patients with moderate to severe ulcerative colitis. *Inflamm. Bowel Dis.* **16**, 1180–1186 (2010).

47. A. Tuin et al., Role of alkaline phosphatase in colitis in man and rats. *Gut* **58**, 379–387 (2009).

48. M. I. Torres, P. Lorite, M. A. López-Casado, A. Ríos, A new approach using tissue alkaline phosphatase histochemistry to identify Crohn's disease. *Pathol. Res. Pract.* **203**, 485–487 (2007).

49. M. Parlato et al., Human ALPI deficiency causes inflammatory bowel disease and highlights a key mechanism of gut homeostasis. *EMBO Mol. Med.* **10**, e8483 (2018).

50. S. Kawamura et al., Plasma membrane-associated sialidase (NEU3) regulates progression of prostate cancer to androgen-independent growth through modulation of androgen receptor signaling. *Cell Death Differ.* **19**, 170–179 (2012).

51. S. Ueno et al., Plasma membrane-associated sialidase is up-regulated in renal cell carcinoma and promotes interleukin-6-induced apoptosis suppression and cell motility. *J. Biol. Chem.* **281**, 7756–7764 (2006).

52. Y. Kakugawa et al., Up-regulation of plasma membrane-associated ganglioside sialidase (Neu3) in human colon cancer and its involvement in apoptosis suppression. *Proc. Natl. Acad. Sci. U.S.A.* **99**, 10718–10723 (2002).

53. D. M. Heithoff et al., Intraspecies variation in the emergence of hyperinfectious bacterial strains in nature. *PLoS Pathog.* **8**, e1002647 (2012).

54. J. Fu et al., Loss of intestinal core 1-derived O-glycans causes spontaneous colitis in mice. *J. Clin. Invest.* **121**, 1657–1666 (2011).

55. S. Narisawa et al., Accelerated fat absorption in intestinal alkaline phosphatase knockout mice. *Mol. Cell. Biol.* **23**, 7525–7530 (2003).

56. L. G. Ellies et al., Sialyltransferase ST3Gal-IV operates as a dominant modifier of hemostasis by concealing asialoglycoprotein receptor ligands. *Proc. Natl. Acad. Sci. U.S.A.* **99**, 10042–10047 (2002).

57. R. F. Goldberg et al., Intestinal alkaline phosphatase is a gut mucosal defense factor maintained by enteral nutrition. *Proc. Natl. Acad. Sci. U.S.A.* **105**, 3551–3556 (2008).

58. K. Ohtsubo et al., Dietary and genetic control of glucose transporter 2 glycosylation promotes insulin secretion in suppressing diabetes. *Cell* **123**, 1307–1321 (2005).

59. N. J. Foot et al., Ndfip1-deficient mice have impaired DMT1 regulation and iron homeostasis. *Blood* **117**, 638–646 (2011).

60. M. R. Davis Jr, J. B. Goldberg, Purification and visualization of lipopolysaccharide from Gram-negative bacteria by hot aqueous-phenol extraction. *J. Vis. Exp.* **63**, 3916 (2012).

61. C. H. Lee, C. M. Tsai, Quantification of bacterial lipopolysaccharides by the purpald assay: Measuring formaldehyde generated from 2-keto-3-deoxyoctonate and heptose at the inner core by periodate oxidation. *Anal. Biochem.* **267**, 161–168 (1999).

62. A. Fuhrer et al., Milk sialyllactose influences colitis in mice through selective intestinal bacterial colonization. *J. Exp. Med.* **207**, 2843–2854 (2010).

Yang et al.
Neu3 neuraminidase induction triggers intestinal inflammation and colitis in a model of recurrent